Journal of Materials Science, Volume 57, Issue 3, January 2022, pp. 1863-1880
DOI:10.1007/s10853-021-06712-5

Optical, structural and morphological studies of nanostructures fabricated on Silicon surface by femtosecond laser irradiation

R. Kuladeep[1,2,#], L. Jyothi[1], Chakradhar Sahoo[1], D. Narayana Rao[1] and V. Saikiran[1,3,*]

[1]School of Physics, University of Hyderabad, Hyderabad, India, 500046.

[2]Welding Engineering and Laser Processing Centre, Cranfield University, Cranfield, Bedfordshire MK43 0AL, England, UK.

[3]Department of Physics, Institute of Science, GITAM Deemed to be University, Visakhapatnam, Andhra Pradesh, India, 530045.

Abstract:

We report here a detailed analysis of the ultrashort laser pulse irradiation effects on a single crystalline silicon surface. A systematic study has been performed to understand the surface morphological changes under irradiation with ultrashort laser pulses by changing different input laser parameters such as laser fluence, laser pulse number, and incident laser polarization. Field emission scanning electron microscopy images reveal the formation of laser induced periodic sub-wavelength surface structures directly on bulk surface. The orientation of the formed sub-wavelength surface structures is perpendicular to the incident laser polarization and their morphology and spatial periodicity strongly depend on the applied laser fluence and laser pulse number. The sub-wavelength surface structures are accompanied by the formation of a large density of silicon nanoparticles which possess broad visible photoluminescence ranging from 410 nm to 680 nm which is due to superficial oxidation of silicon during laser irradiation. The amount of oxygen incorporated into silicon strongly depends on laser parameters such as laser fluence and number of laser pulses.

Keywords: femtosecond laser; laser-induced periodic surface structures; LIPSS; silicon nanostructures; photoluminescence;

Corresponding Email: *svadaval@gitam.edu

#kuladeepaug13@gmail.com & kuladeep.rajamudili@cranfield.ac.uk

1. Introduction

Silicon (Si) is a key semiconductor material having important technological applications both in photonics and microelectronics owing to the low cost and feasible incorporation of Si into diverse devices. Different forms of Si like amorphous, nanocrystalline, and porous have been used for different types of applications such as solar cells, photonics, and electronics [1-5]. Still, Si is a poor light emitter and cannot be used to detect many important communications wavelengths because of its indirect band gap [6]. Since last two decades a lot of large-scale research is going on towards manipulating the properties of Si by different methods for utilization in different applications [7-9]. Surface processing by using ultrashort laser pulses is one such important method over others which has received significant attention over the past few years because ultrashort lasers interact directly with any kind of material and then melt, ablate and alter their surfaces for a wide variety of applications [10-15]. Ultrashort laser treatment of materials has advantages like the reduction of the heat-affected areas and rapid energy delivery when compared to the effects induced by longer pulsed lasers, which makes the usage of ultrashort lasers as a potential tool in the material processing at micro and nanoscale [16]. It has been widely reported that during the ultrashort laser interaction with the material laser-induced periodic surface structures (LIPSS) or ripples are formed on the surface of a material. Different researchers have reported the fabrication of LIPSS on a variety of materials with potential applications of the fabricated nanostructures for micro-fluidics [17, 18], nanogratings for antireflection coatings [19, 20], colorization of metals [21] and substrates for the detection of biomolecules and explosives by the tool surface-enhanced Raman scattering (SERS) [22-25].

Coming to the interaction of ultrashort laser pulses with Si different reports are available to date [26-30]. The specific phenomena of LIPSS formation on Si surface have been studied by varying different input laser processing parameters like incident laser wavelength, laser fluence, laser beam profile, pulse duration, number of incident laser pulses, angle of incidence, and laser polarization. The LIPSS are in general formed under single or multiple laser pulses irradiation at low fluence around the ablation threshold, where the ripples have their wave vectors parallel to the laser *E*-field, and the ripple period strongly depends on the incident laser wavelength [31-33]. It is observed that the spatial periodicity of the ripples strongly depends on the dielectric medium that surrounds the material [34]. The LIPSS formation on Si by ultrashort laser irradiation and the dependence on different laser parameters

as well as the surrounding dielectric medium is well reported. But the theoretical understanding is still under debate. Lee et.al, have recently proposed a mask-free patterning method of Si by combining the conventional wet chemical etching process with ultrashort laser direct writing LIPSS patterns on Si surface [35]. Nivas and coworkers have studied the formation of LIPSS on Si by irradiating Si with laser in atmosphere and in high vacuum and highlighted the oxygen ambience in the air plays an important role in the surface ripple formation [36]. Ionin and their group have reported that the periodic nanostructures grow from subwavelength to micron sizes with wavelength, fluence, exposure time of the irradiating laser [37]. In another report they have shown that structural modification occurs in the deep subsurface of Si due to ultrashort intense laser irradiation and this formation is attributed to inhomogeneous ablation in valleys of surface ripples and formation of different polymorphs of crystalline Si embedded in amorphous Si [38]. The formation of microstructures within the laser spot on the Si irradiated with femtosecond optical vortex beam and their dependence on the laser fluence was also reported earlier [39]. Even though there were many reports available on the formation of LIPSS on Si surface for various applications still there are gaps like the analysis of the structure of LIPSS, the modifications observed in the surrounding area of the laser irradiated position on Si surface, influence of the debris collected during irradiation on the LIPSS formation and their luminescence characteristics and formation of fine structured LIPSS. In this report, we investigate thoroughly these gaps with an elaborate analysis on the influence of different laser input parameters in the formation of LIPSS on Si surface under ultrashort laser irradiation of Si surface in ambient air atmosphere. We have also investigated the structural and optical properties of the laser fabricated nanostructures on silicon surface with various laser parameters.

2. Experimental details

P-type (10–20 Ω cm) (1 1 1) Si wafers have been used for the laser irradiation experiments. Prior to that the Si wafers have been etched with 8% hydrofluoric acid for 5 min to remove the native oxide layer on the surface. The Si samples were irradiated by multiple (N) femtosecond laser pulses in an ambient air environment. The laser source utilized in irradiation experiments was a Ti:Sapphire oscillator-amplifier system (Spectra Physics, Spitfire) operating at a wavelength of ~ 800 nm and delivering ~ 1 mJ output energy pulses at a repetition rate of 1 kHz. Duration of each laser pulse was about ~ 110 fs. The fs laser pulses are linearly polarized. Neutral density filters and the combination of half wave plate and a polarizer have

been utilized to adjust the irradiation fluence. The laser beam is made to incident normal to the Si surface and focused with the help of a microscopic objective lens of numerical aperture of 0.25 and writing is performed transverse to the laser propagation direction. In order to account for the reflection losses of the lens all the energy/fluence measurements were performed after the lens. Computer controlled translational stages (Newport, USA) were arranged to translate the sample in x, y, and z directions. Scanning of the sample was done in both along and normal to the laser polarization direction. Several variable parameters such as laser fluence (*F*), number of incident laser pulses (*N*), and polarization of the incident laser pulses are involved in the experimentation. We examine the extent to which these parameters affect the final morphology and chemical composition of the laser irradiated surface. Detailed characterization of the morphological changes, structural properties, and chemical composition of the Si surface after laser irradiation have been performed by field emission scanning electron microscope (FESEM), micro-Raman spectroscopy, and energy dispersive X-ray analysis (EDAX) associated with FESEM, respectively. The EDAX measurements are performed with electron accelerating voltage of 20 kV and the beam is scanned normally on the sample surface.

3. Results and Discussion

Morphology of the irradiated Si surface:

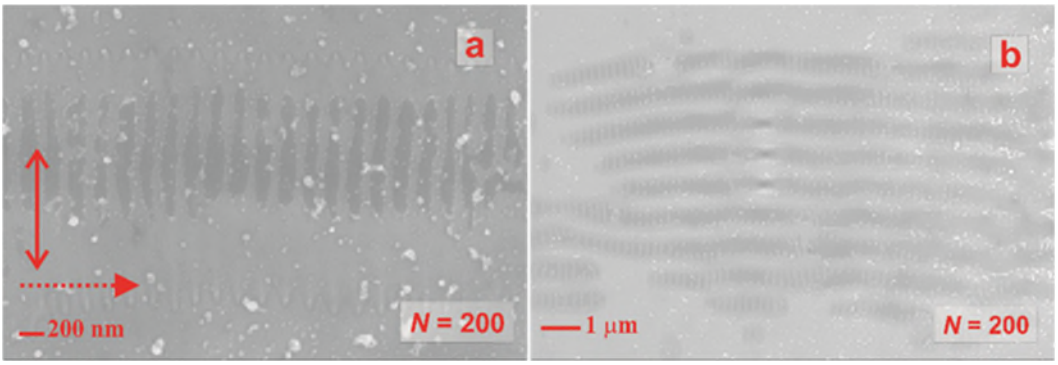

Figure 1. Surface morphology of Si surface after irradiation with fs laser pulses in air with (a) F = 0.22 Jcm^{-2} and (b) F = 0.26 Jcm^{-2} fluence respectively. Solid and dashed arrow in figure 1(a) represents direction of the laser polarization and the direction of sample translation respectively.

Figure 1 shows FESEM images of the structures directly written on the Si surface by a single scan along the +X direction in the air as a function of a superimposed shot number of linearly polarized fs laser pulses *N* at various irradiation fluences *F* respectively. The

spontaneous nature of LIPSS inside the features results from the enhanced near-field due to the excitation of surface plasmons, which was discussed in the next section. Spatial periodicity (Λ) of LIPSS is significantly smaller than laser wavelength and two different kinds of periodic gratings have been noticed for the range of laser fluences and irradiated number of pulses (scanning speeds) on the Si surface. The first one corresponds to periods less than 320 nm which was assigned as high spatial frequency LIPSS (HSFL) or deep sub-wavelength ripples where the ratio of Λ to the laser wavelength (λ), at normal incidence is lower than 0.4. On the other hand, sub-wavelength periodic features with periods between 320 nm and 800 nm, namely low spatial frequency LIPSS (LSFL) or near sub-wavelength ripples appear with Λ/λ ratio values between 0.4 and 1.0. Figure 1(a) shows the formation of HSFL features which are aligned parallel to the incident laser beam polarization under the lower fluence of $F = 0.22$ Jcm^{-2}. Under irradiation with the fluence of $F = 0.26$ Jcm^{-2} coexistence of LSFL features oriented perpendicular to the laser polarization and HSFL features along the laser polarization are observed as shown in figure 1 (b). Decreasing the pulse number ($N < 200$ i.e., by increasing the scanning speed) at both these fluences we didn't observe any surface texturing on Si and the threshold fluence for the modification of Si surface is found to be 0.2 Jcm^{-2}. Spatial periodicity (Λ) of HSFL and LSFL features is found to be 220 ± 5nm and 770 ± 20 nm, respectively.

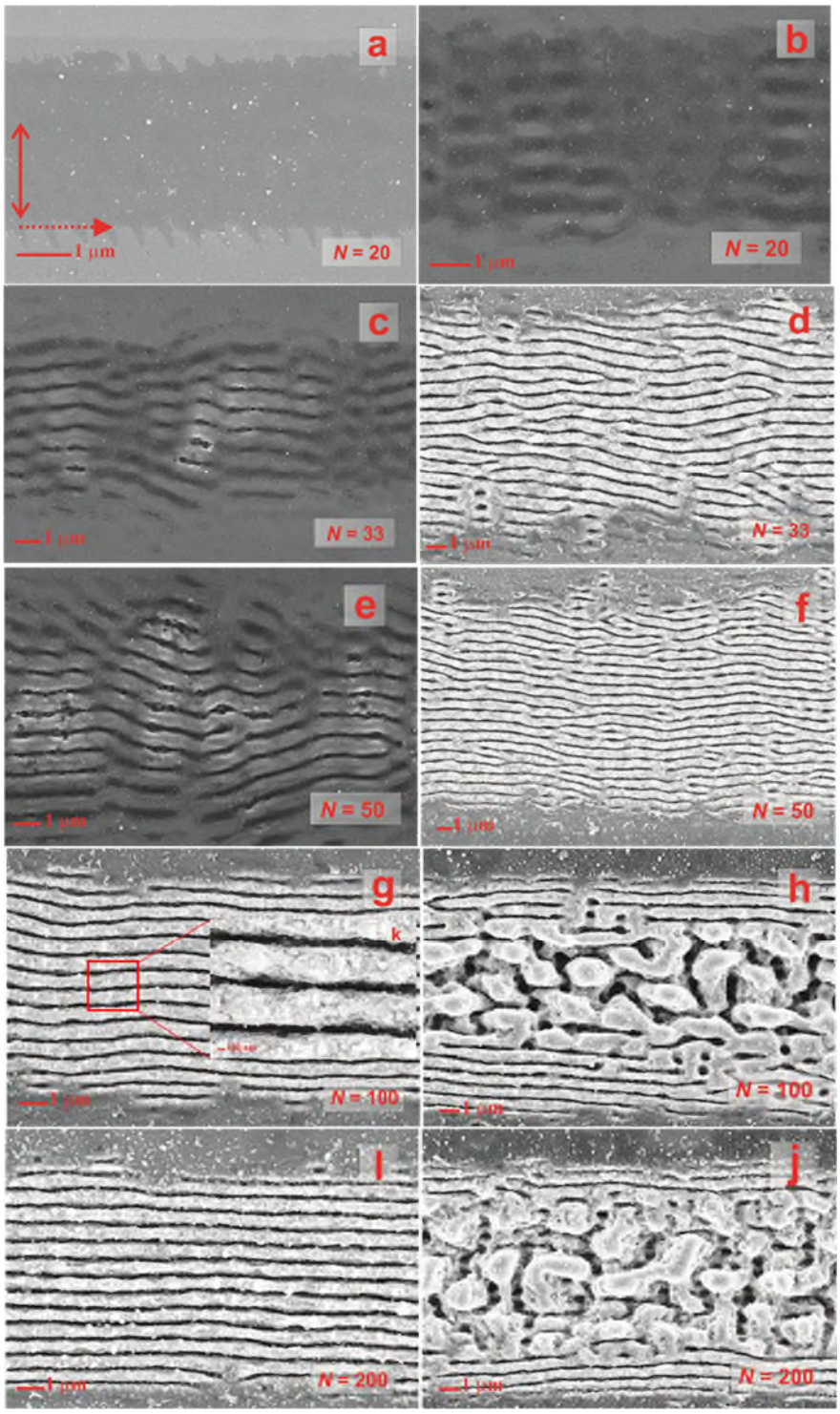

Figure 2. FESEM images of Si surface in air after irradiation with fs laser pulses. Figures (a), (c), (e), (g) and (i) are written with laser fluence of 0.3 Jcm^{-2}; (b), (d), (f), (h) and (j) are written with laser fluence of 0.42 Jcm^{-2}. Figure 2(k) shows magnified FESEM image of laser induced periodic features of figure 2(g). Applied number of laser pulses is labeled on the images, laser polarization and writing directions are indicated by the solid and dotted arrows, respectively in figure 2(a).

At higher laser fluence, between 0.3 and 0.5 Jcm^{-2} surface morphology was found to be dependent on the pulse number and we noticed three main stages of ripple dynamics: primary random nanoroughness (formation of nanoparticles), ripple formation (sub wavelength features), and grooves formation. The nanoroughness is found to emerge with the initial laser pulses N = 20 under the irradiation of both the fluence 0.3 and 0.42 Jcm^{-2} as shown in figure 2 (a) and (b). Repetitive irradiation of such random nanoroughness results in the appearance of LIPSS with periods in the range $0.7\lambda < \Lambda < \lambda$. Features in Figures 2(a), 2(c), 2(e), 2(g) and 2(i) are fabricated with laser fluence of 0.3 Jcm^{-2}, while figures 2(b), 2(d), 2(f), 2(h) and 2(j) are fabricated with 0.42 Jcm^{-2}, with different number of pulses respectively. As can be seen in figures 2(c) and 2(e) LSFL features which are discontinuous in nature are formed under irradiation of N = 33 and 50 pulses of 0.3 Jcm^{-2} fluence. Under the irradiation with 0.42 Jcm^{-2} fluence for N = 33 and 50 we observed the formation of LSFL all over the visible laser modified region as shown in Figures 2(d) and 2(f), on further increasing the applied number of pulses, some aperiodic structures develop in the centre of the visible laser modified region, while long continuous LSFL are formed along the edges of the both sides of laser modified region for N = 100 and 200 as shown in the Figures 2(h) and 2(j). But with the lower fluence of 0.3 Jcm^{-2} for N = 100 and 200 regular and continuous LSFL are formed all over the laser modified region as shown in the Figures 2(g) and 2(i). The spatial separation of the LSFL features are found to decrease from 770 to 560 nm by varying the parameters like fluence from 0.2 to 0.5 Jcm^{-2} and number of laser pulses, indicating decrease in periodicity with increase in fluence and also with increase in the number of applied laser pulses. Figure 2(k) shows a magnified FESEM image of laser induced periodic ripples of figure 2(g).

Upon further increase of fluence, another characteristic feature of few-µm sized grains develops all over the laser modified region as shown in Figure 3 which is fabricated with a fluence of F = 0.65 Jcm^{-2} and N = 100. Figure 3(b) & (c) are the magnified images of Figure 3(a) which show the formation of nanoparticles (NPs) inside the grains.

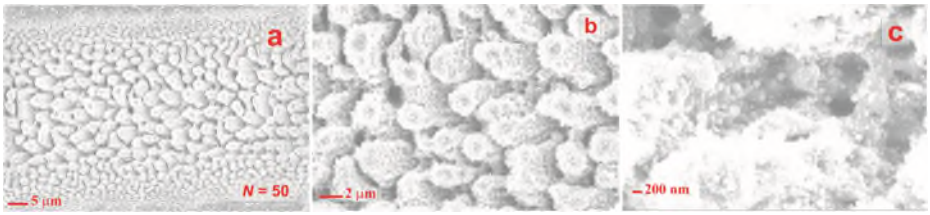

Figure 3. (a) FESEM micrographs of Si surface in air after irradiation with laser fluence of 0.65 Jcm^{-2}. (b) and (c) represents high resolution images of (a).

In general, the investigated LSFL are oriented nearly perpendicular to the laser polarization, which is a remarkable characteristic for such an ultrafast laser induced nanostructures. When we rotated the laser polarization from $\theta = 0°$, $\theta = 45°$, $\theta = 90°$ and $\theta = 135°$, orientations of LSFL were found to be rotated by $\theta = 0°$, $\theta = 45°$, $\theta = 90°$ and $\theta = 135°$, accordingly. In addition, our results with vertical and horizontal scanning of Si demonstrate that the scanning direction have no influence on the surface morphology and orientation of LSFL. These results are shown schematically in figure 4, which were fabricated with fluence of a $F = 0.3$ Jcm^{-2} and $N = 100$. These observations indicate that the formation and arrangement of LIPSS were strongly ~~related to~~ dependent on the polarization of laser light and independent of sample scanning direction.

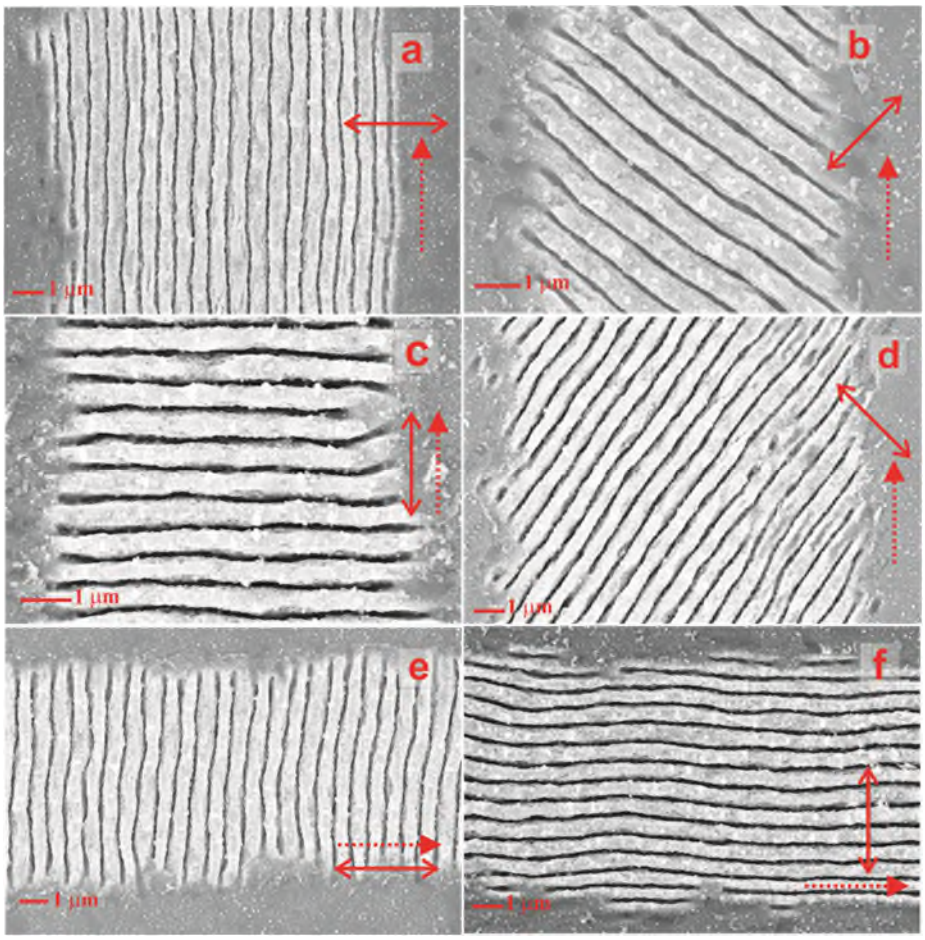

Figure 4. (a) FESEM micrographs of LIPSS on Si surface after irradiation in air with laser fluence of $F = 0.3$ Jcm^{-2} and $N = 100$ pulses with different polarization directions and writing directions. Laser polarization and writing directions are indicated by the solid and dotted arrows, respectively.

Structural and optical properties of femtosecond laser excited Silicon

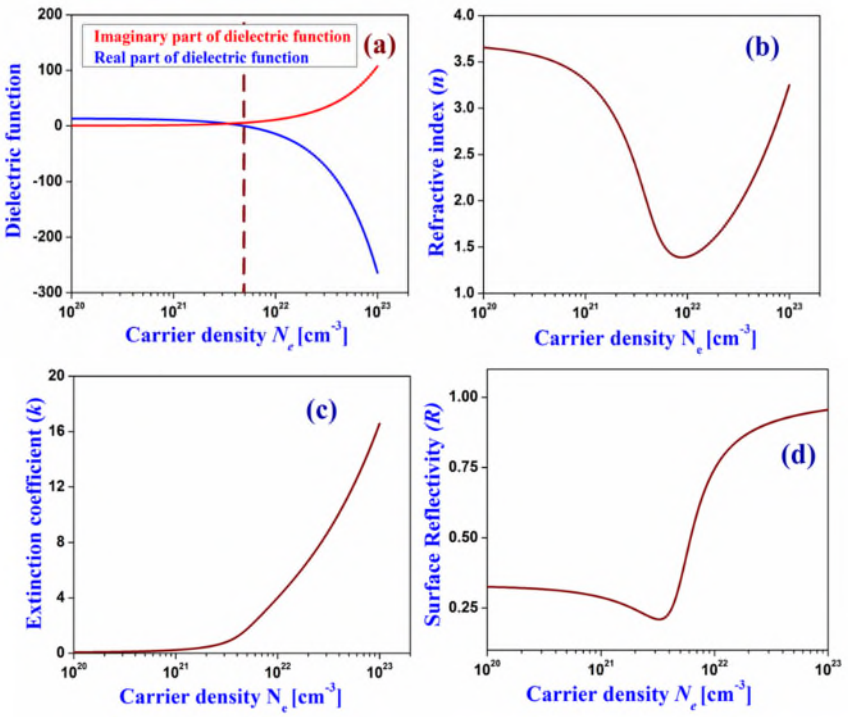

Figure 5. Optical properties of fs laser irradiated single-crystalline silicon as a function of the excited carrier densities N_e for the irradiation wavelength of 800 nm. (a) Real and imaginary parts of dielectric function, dotted line in the plots indicates the critical carrier density above which the Si surface exhibits a sharp transition from semiconductor to metallic nature, (b) Refractive index n(N_e), (c) Extinction coefficient k*(N_e) and(d) Surface reflectivity R*(N_e).*

Under irradiation of femtosecond laser pulses on Si surface, electrons will be excited from the valence band to the conduction band through linear and two-photon absorption processes [40]. As the excitation takes place at a much shorter time than the electron-phonon relaxation time, free electron density N_e in the conduction band increases by laser irradiation. The changes in the dielectric function due to the generation of free carriers in the conduction band of the material can be described by the below equation according to Drude model [41], Band-filling effect and renormalization of the band structure are neglected here

$$\Delta\varepsilon_{Drude} = \frac{-e^2 N_e}{\varepsilon_o\, m_e m_{opt}\, \omega^2} \frac{1}{\left[1 + \frac{i}{\omega\tau_D}\right]} \quad (1)$$

where e is the charge of the electron, m_e free electron mass, ε_o is the vacuum dielectric permittivity, ω optical angular frequency, τ_D is the Drude damping time, m_{opt} is the optical effective mass of the carriers and N_e is the free carrier density under fs laser irradiation.

The complex dielectric function of the fs laser excited Si surface ε^* is expressed as the following equation with the Drude term (free carrier response) added to the dielectric function of unexcited Si (ε) [42]

$$\varepsilon^* = (n^* + i\,k^*)^2 = \varepsilon + \Delta\varepsilon_{Drude}$$

$$\varepsilon = (n + i\,k)^2 = \varepsilon_r + i\varepsilon_i$$

Where n* and n is the refractive index, k* and k is the extinction coefficient of the laser excited Si surface and unirradiated Si surface respectively.

Real and Imaginary parts of the dielectric function of fs laser irradiated surface as a function of free carrier density are expressed as

$$\varepsilon_r^*(N_e) = \varepsilon_r - \frac{e^2 N_e \tau_D^2}{\varepsilon_o\, m_e m_{opt}\, \omega^2 [1 + \omega^2 \tau_D^2]} \quad (2)$$

$$\varepsilon_i^*(N_e) = \varepsilon_i + \frac{e^2 N_e \tau_D}{\varepsilon_o\, m_e m_{opt}\, \omega [1 + \omega^2 \tau_D^2]} \quad (3)$$

Refractive index, extinction coefficient and surface reflectivity of the laser irradiated Si surface are expressed as

$$n^*(N_e) = \sqrt{\frac{\varepsilon_r^*(N_e) + \sqrt{\varepsilon_r^*(N_e)^2 + \varepsilon_i^*(N_e)^2}}{2}} \quad (4)$$

$$k^*(N_e) = \sqrt{\frac{-\varepsilon_r^*(N_e) + \sqrt{\varepsilon_r^*(N_e)^2 + \varepsilon_i^*(N_e)^2}}{2}} \quad (5)$$

$$R^*(N_e) = \frac{(n^*(N_e) - 1)^2 + k^*(N_e)^2}{(n^*(N_e) + 1)^2 + k^*(N_e)^2} \quad (6)$$

Excitation dependent behavior of the optical properties of the fs laser excited Si surface as a function of N_e is shown in figure 5. Figure 5(a) shows the real and imaginary parts of the

dielectric function calculated by using Eqs, (2) and (3), figure 5(b) and 5(c) illustrates corresponding refractive index [$n^*(N_e)$] and extinction coefficient [$k^*(N_e)$] which are calculated by using Eqs. (4), (5) and 5(d) show the surface reflectivity [$R^*(N_e)$] as function of N_e calculated by Eq (6) can been seen in figure 5(d).

As shown in figure 5(a) with the increase in the carrier concentration, the real part of the dielectric function of the fs laser excited Si surface decreases and above a particular carrier density called as critical carrier density ($N_{cr} = 4.8 \times 10^{21}$ cm^{-3}) it becomes negative, which means that semiconductor virtually becomes a metal and such a process is called as non-thermal phase transition [43]. Hence the fs laser generated free-electron plasma induces a sharp transition from semiconductor to metallic behaviour. Refractive index and the extinction coefficient of the laser-excited silicon surface both significantly depend on the carrier densities. Starting from the values of non-excited Si, for increasing N_e, the refractive index exhibits a minimum before it increases again as shown in figure 5(b). Similarly, a strong carrier-dependent behavior of the extinction coefficient can be seen in figure 5(c). Transparent Si surface under lower electron density starts absorbing the incident radiation with the increase in the carrier concentration as shown in figure 5(c). Simultaneously, the surface reflectivity of the fs laser excited Si surface under normal incident radiation increases significantly during the transition from semiconductor to a metallic nature as shown in figure 5(d). From these observations, we can comment that due to the excitation of the valence band electrons to conduction band with fs laser irradiation, the surface of fs laser irradiated Si changes into a highly reflective metal like behavior from a semiconductor like behavior, which is famously known as non-thermal phase transition [43]. It was described that the surface irradiated with short pulsed laser with damage threshold fluence will behave like a metallic surface, no matter for metal, semiconductor or dielectric surface which supports the surface Plasmon generation [44].

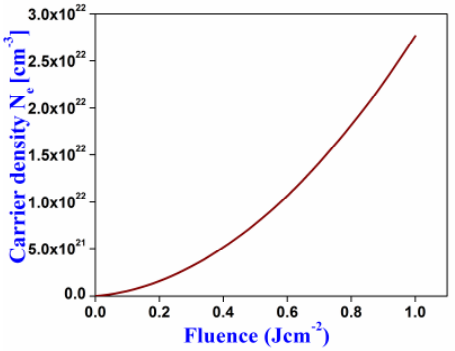

Figure 6. Carrier density of fs laser irradiated single-crystalline silicon as a function laser fluence under normal incidence.

Under fs laser irradiation the carrier density in the conduction band of silicon can be estimated as a function of the laser fluence using a model that considers linear and two-photon absorption [41]

$$N_e(\phi_0) = \frac{\phi_0(1-R)}{h\nu}\left\{\alpha + \beta\phi_0 \frac{(1-R)}{2t_o\sqrt{2\pi}}\right\} \quad (7)$$

Where α is the linear absorption coefficient, β is the two-photon absorption coefficient, R is the surface reflectivity, ν is the frequency of incident radiation, h is the Planck constant and t_0 is the pulse duration of the incident radiation. Carrier density as a function of laser fluence under normal incidence is shown in figure 6, which was plotted using Eq (7). Optical and physical constants have been used from literature [41, 42]. A metallic surface gives rise to the possibility of exciting surface plasmons which are the excitation of longitudinal charge density oscillations. The interference of the incident laser light and the generated surface plasmons cause a periodic modulation of the surface. Light can be coupled into SPPs from free space only by matching the momentum of the SPPs. Surface plasmons cannot be generated as the surface plasmon momentum always exceeds the incident light momentum [42, 45, 46]. As shown in figure 2(a) and (b) under irradiation with initial laser pulses (N = 20) at both the fluences of 0.3Jcm^{-2} and 0.42 Jcm^{-2}, the rapid localized energy deposition followed by a rapid expansion and cooling of Si surface can result in nano-particle generation [47, 48] making the surface irregular. Repetitive irradiation of such a roughness results to the nano-ripple formation due to the excitation of the surface plasmons at the roughened Si surface by the incident laser light [49-51]. Hence, a roughness of appropriate periodicity that satisfies the quasi-momentum matching condition [52] must be satisfied and is given by

$$k_s - k_i \sin\theta = G \quad (8)$$

Where k_s is the wave vector of surface plasmon ($k_s = 2\pi/\lambda_s$), k_i is the wave vector of incident laser ($k_i = 2\pi n \sin\theta/\lambda_i$), where λ_i is the incident laser wavelength, n is the refractive index of the ambient medium, and $|G|$ is the quasi-momentum provided by the surface roughness. On further irradiation laser interacts with the surface of enhanced roughness giving rise to the formation of grating like LSFL surface (random nano-structures) in which ripples are discontinuous and anisotropic in nature as can be seen in figure 2(c) and 2(e), which is due to the weak excitation of surface plasmons [44]. It is known that both localized and propagating surface plasmons along a surface can be excited by coupling laser light to nanostructures. Garrelie et al. experimentally demonstrated the effect of an initially structured surface on the SPP generation

which gives the experimental evidence of grating assisted surface plasmon laser coupling [33]. On increasing the number of laser pulses, grating-assisted surface plasmon-laser coupling occurs, which results in the deepening of ripples. Thus due to grating-assisted surface plasmon-laser coupling long continuous LSFL are observed all over the laser modified region with 0.42 Jcm^{-2} fluence for N = 33 and 50 (figures 2(d) and 2(f)), whereas with a lower fluence of 0.3 Jcm^{-2} for N = 100 and 200 (figures 2(g) and 2(i)) regular and long continuous ripples are observed. Bonse et al explained theoretically and experimentally that the appearance of LSFL depends on the density of generated carriers in the conduction band of the laser excited silicon, which were formed only in a relatively narrow range of laser generated carrier concentration (which corresponds to laser fluence) and at a higher density of generated carriers the LSFL feature vanishes [52]. Our experimental results also show that formation of LSFL are only possible with fluences ranging between 0.3 and 0.5 Jcm^{-2} (with appropriate pulse number) all over the laser modified region and at a higher fluence of 0.65 Jcm^{-2} (which is greater than the single-pulse ablation threshold, [53] LSFL are not observed anymore in the laser modified region where a threshold for generated carrier density for the formation of LSFL is exceeded.

The spatial periodicity of the ripples depends on the angle of incidence, laser wavelength, refractive index of the ambient medium and surface plasmons (which depends on the carrier density of the irradiated Si surface).

From Eq 8 we have

$$\frac{2\pi}{\lambda_s} - \frac{2\pi\mu\sin\theta}{\lambda_i} = \frac{2\pi}{\Lambda}$$

Spatial period (Λ) of the ripples formed by the interference of laser with SPPs is expressed as

$$\Lambda = \frac{\lambda_i}{\frac{\lambda_i}{\lambda_s} - \mu\sin\theta} \qquad (9)$$

In the present study laser is incident normally (i.e., $\theta = 0^0$) on the silicon surface therefore the spatial period can be expressed as

$$\Lambda = \lambda_s = 2\pi \big/ \mathrm{Re}(k_s)$$

Where $$k_s = k_i \sqrt{\frac{\varepsilon^* \varepsilon_d}{\varepsilon^* + \varepsilon_d}} \qquad (10)$$

$\mathscr{E}^*$ is the dielectric constant of the fs laser excited Si surface and $\mathscr{E}_d$ is the dielectric constant of the surrounding medium. Hence spatial periodicity of laser induced ripples depends on the dielectric function of laser irradiated Si surface and surrounding dielectric medium (air in the present study) and is given by

$$\Lambda = \lambda_s = \lambda_i \sqrt{\frac{\left(\varepsilon_r^*(N_e) + \varepsilon_d\right)^2 + \varepsilon_i^*(N_e)^2}{\varepsilon_d\left\{\varepsilon_r^*(N_e)\left(\varepsilon_r^*(N_e) + \varepsilon_d\right) + \varepsilon_i^*(N_e)^2\right\}}} \qquad (11)$$

Where $\mathscr{E}_r^*(N_e)$ and $\mathscr{E}_i^*(N_e)$ are the real and imaginary parts of the dielectric constants of the fs laser irradiated Si surface.

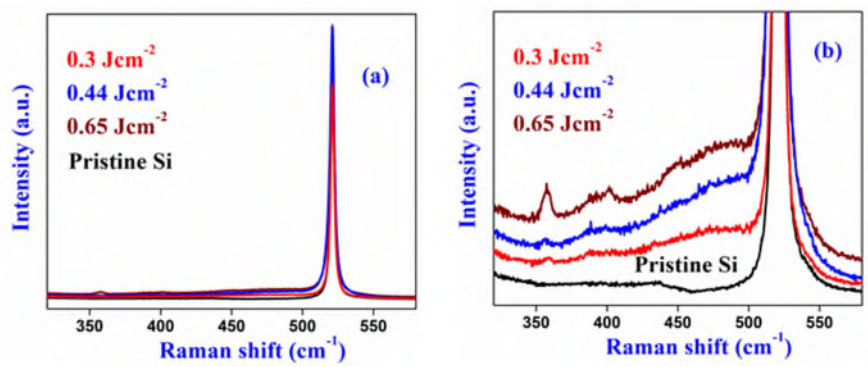

Figure 7: Raman spectra of pristine and fs laser irradiated Si surface.

To understand the structural changes in the fs laser irradiated Si surface micro-Raman spectroscopy has been utilized as this method is very important and nondestructive to measure the structural changes induced in Si [56-59]. The Raman spectra of pristine and laser irradiated Si have been recorded using micro-Raman spectrometer (model LABRAM-HR) with a 632 nm wavelength as the excitation wavelength under similar conditions. Figure 7(a) shows micro-Raman spectra between 200 and 800 cm^{-1} of reference spectrum of non-irradiated single-crystalline Si surface along with surfaces irradiated with F = 0.3, 0.41, and 0.64 J/cm^{-2}. For comparison resolution of the vertical axis of figure 7(a) has been increased as shown in figure 7(b) and each spectrum was shifted vertically. The spectrum is dominated by the narrow 520.5 cm^{-1} mode, arises from the first-order Raman scattering of the longitudinal optical (LO) and the transverse optical (TO) phonon modes. In addition to the band at 520.5 cm^{-1}, a broad band around 475 cm^{-1} can be seen in the laser irradiated Si surfaces, which is attributed to first-order scattering of vibrational TO phonon modes of amorphous silicon (a-Si), which is a characteristic feature of a-Si arising due to the formation of a thin amorphous top-layer due to

the fs-laser irradiation [60-62]. The asymmetry towards the lower wavenumber side indicates the modifications in the laser irradiated region which are attributed to the nanostructured Si formed as a result of irradiation. A Broad peak observed at 357 cm^{-1} is due to the presence of some other high pressure phases of Si which are more predominantly observed in the high fluence irradiated samples [39]. This indicates that new high pressure phases are embedded in the nanostructures formed after high fluence irradiation. Thus, Raman spectra reveal the formation of a thin amorphous layer on a crystalline Si and a formation of high pressure phases under the fs-laser irradiation with the variation in irradiation fluence.

Silicon oxidizes instinctively in air to form a thin native oxide layer of thickness around few nm. Oxidation happens via direct reaction of oxygen atoms or molecules with the surface atoms. Under laser irradiation in an oxygen-rich atmosphere (air) surface oxidation of silicon is a well-known phenomenon [63-67]. Laser irradiation enhances the diffusion of oxygen into the silicon substrate gives rise to surface oxidation of Si. 1μm thick oxide layers have been reported using laser-enhanced oxidation of silicon surfaces [67].

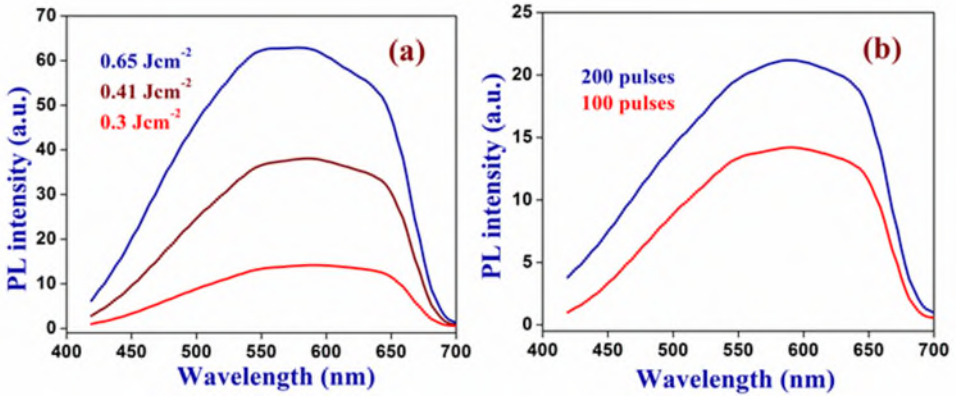

Figure 8: Photoluminescence spectrum of fs laser irradiated silicon surface under the excitation of 365 nm wavelength. (a) Function of laser fluence (F) used to irradiate the silicon surface and (b) function of laser pulses (N) with fluence F = 0.3 Jcm^{-2} used to irradiate the silicon surface

We obtained strong photoluminescence (PL) which covers almost entire visible region (430-680 nm) from fs laser irradiated Si surface in air due to the presence of a large amount of oxidized Si nanoparticles. PL spectra are recorded in a confocal geometry distinguishing the laser irradiated region to the rest of the Si wafer by exciting the sample with 365 nm wavelength. Luminescence is collected in the wavelength range from 400 to 700 nm within and around the laser irradiated region. All the measurements were performed at room

temperature. Figure 8(a) shows the PL spectra of the samples irradiated with 0.3, 0.44, and 0.65 J/cm^2 fluence and N = 100 pulses respectively. The peak wavelength, which is approximately 580 nm, is the same for all the three samples irradiated with the same number of laser pulses N but with different fluences, and the peak luminescence intensity increases with increasing the laser fluence. Figure 8(b) shows the PL spectra of the samples irradiated with N = 100 and 200 pulses and 0.3 J/cm^2 fluence. It is observed that peak luminescence intensity increases with an increase in the irradiation number of laser pulses. The PL emission properties of fs laser irradiated Si surface that are observed are most likely due to the oxidation of Si surface under fs laser irradiation. Further fluorescence microscopy imaging which displays the fluorescence images collected by excitation at 365 nm are shown in figure 9. Figure 9(a) shows the fluorescence image of laser irradiated Si surface with F = 0.3 Jcm^{-2} fluence and N = 200 pulses in full spectral range configuration and the corresponding FESEM image of surface morphology of Si surface is shown in inset. Selected spectral range fluorescence microscopy images (wavelengths labeled in the images) of the irradiated Si surface are shown in the figures 9 (b)-(e). Figure 9(f) corresponds to the selected spectral range fluorescence image of Si surface irradiated with F = 0.65 Jcm^{-2}, which also shows the emission from debris surrounding the fabricated microstructure.

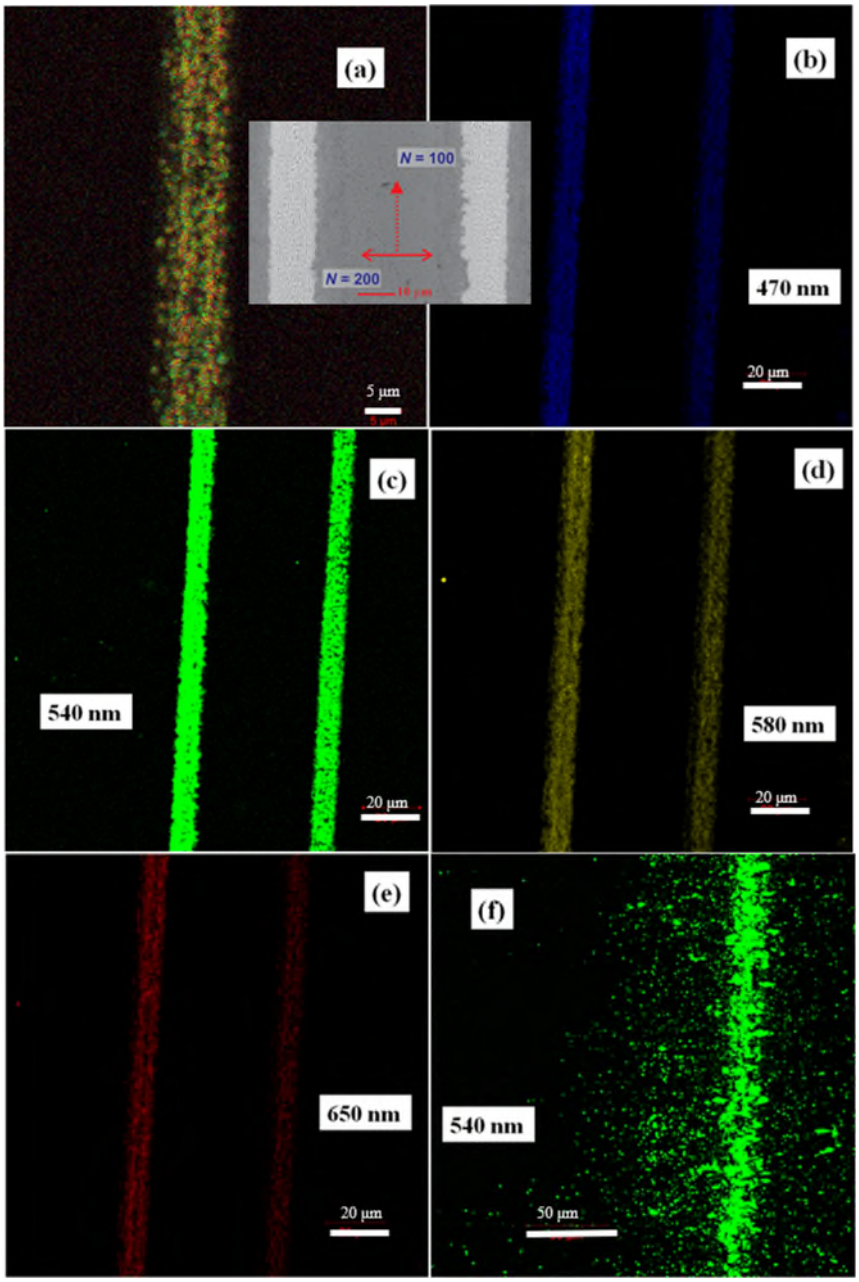

Figure 9: Fluorescence imaging microscopy of fs laser irradiated silicon surface. (a) Full spectral range fluorescence image of microstructure fabricated with F = 0.3 Jcm^{-2} and N = 200 pulses. (b), (c, (d) and (e) corresponds to fluorescence images selected at four different wavelengths of the microstructures fabricated with fluence F = 0.3 Jcm^{-2} using N = 100 and 200 pulses. (f) Fluorescence image of the microstructure fabricated with fluence of F = 0.65 Jcm^{-2}.

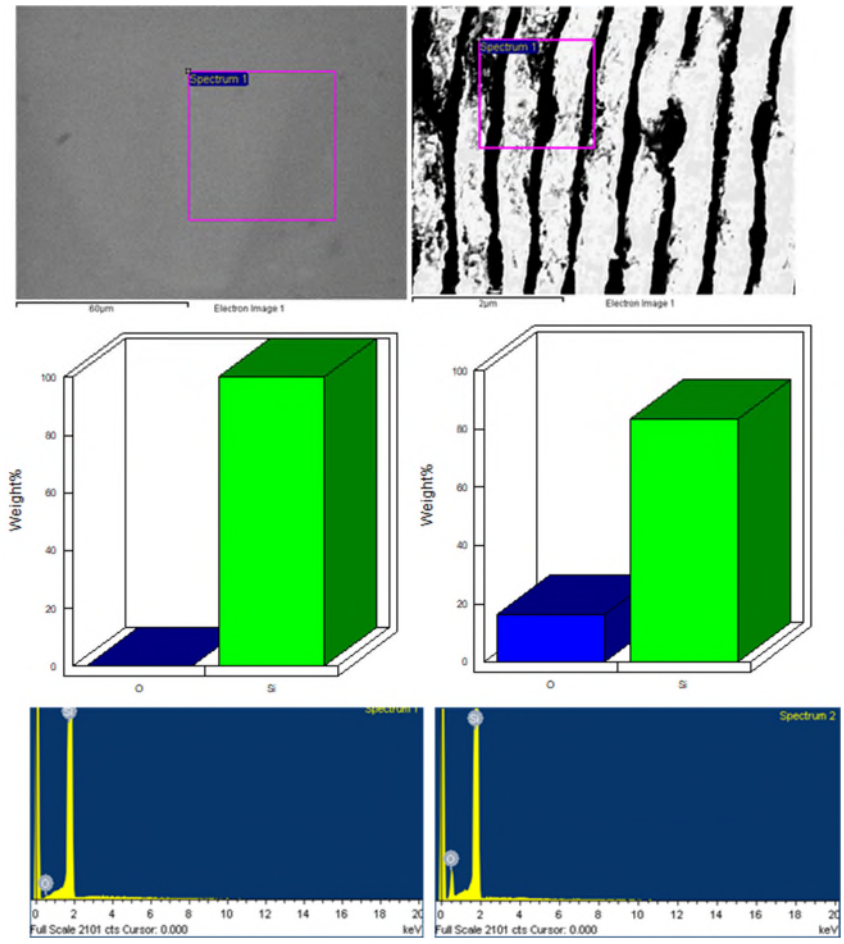

Figure 10: EDX measurements on unirradiated and fs laser irradiated silicon surface. Square shaped marked area indicates the region where EDX measurements were performed.

To determine the origin of the photoluminescence, we analyzed the chemical composition of the laser irradiated Si surface by using Energy dispersive X-ray spectroscopy (EDX). EDX spectra of pristine Si and laser irradiated Si (with fluence of F = 0.3 Jcm^{-2}) surfaces are shown in figure 10. EDX spectra obtained from laser irradiated region (with fluence of F = 0.3 Jcm^{-2}) show only Oxygen and Silicon peaks, whereas from the pristine Si surface no oxygen signal is observed. It is also observed that as the pulse number N or fluence F increases, the intensity of oxygen signal increases, while the Si signal is decreased, as shown in figure 11 indicating that the amount of oxygen incorporated into the Si surface increases with increasing N or F. Increase in the amount of oxygen content may correspond to a higher atomic ratio of oxygen to silicon. These results indicate superficial oxidation of silicon surface upon irradiation with fs laser pulses in air. As reported earlier under laser irradiation in oxygen-rich atmosphere surface oxidation takes place due to diffusion of oxygen into melted Si during irradiation [63-67]. The diffusion coefficient of oxygen in liquid silicon is six orders of

magnitude greater than that in solid silicon [67]. The greater the oxygen to silicon ratio that we observed from the samples irradiated at higher fluence may therefore be attributed to a large increase in the surface temperature. From the EDX analysis it is clearly evident that the presence of oxygen impurities on the fs laser irradiated silicon surface and the increase of both the oxygen to silicon ratio and luminescence intensity with laser fluence (*F*) or applied number of laser pulses (*N*) demonstrates that the PL emission comes from the oxidized silicon on the fs laser structured silicon surface. Results of luminescence from the sample after etching support this hypothesis, when an fs laser irradiated silicon surface is etched in 8% hydrofluoric acid (HF) solution for about 10 min, the PL disappears. Figure 11 (c) shows the effect of etching on photoluminescence from the laser irradiated silicon surface. Practically no photoluminescence could be observed from the laser irradiated region after etching in HF. In addition, it was reported that the silicon surface irradiated in a vacuum will not show any photoluminescence [63].

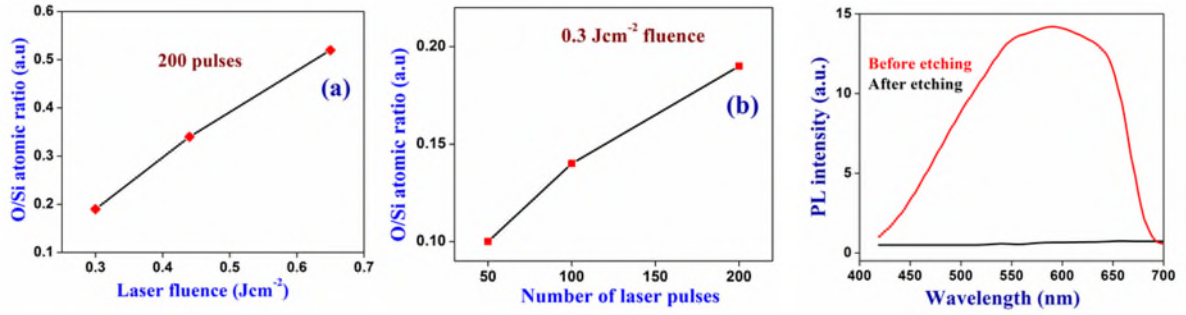

Figure 11: The atomic ratio of oxygen to silicon in silicon microstructures induced by femtosecond laser (a) with different fs laser fluences and N = 200 pulses and (b) with different number of laser pulses N and a laser fluence of 0.3 Jcm^{-2}. (c) Etching effect on the photoluminescence of femtosecond laser irradiated silicon surface.

Effect of debris on the formation of periodic structures on Si surface:

Formation of sub-wavelength structures at the irradiated region of Si surface is accompanied by a significant amount of debris in and around the laser irradiated region. In order to obtain information about microscopic properties such as size, shape, and chemical composition of microparticulates, situated in and around the ablated regions the formed debris is analyzed by using different techniques including FESEM and TEM.

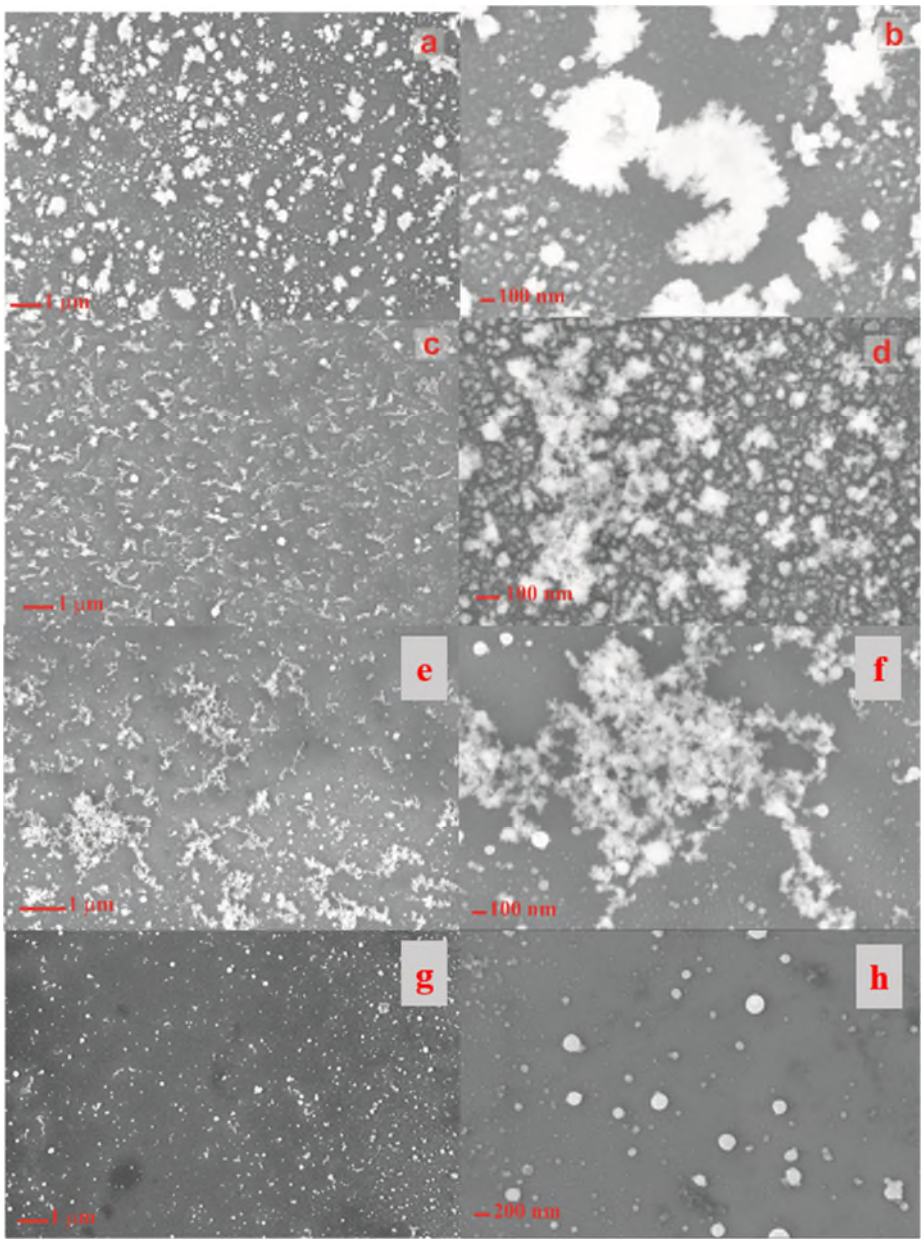

Figure 12: FESEM micrographs (under different magnifications) showing the morphology of Si debris formed on the surface under irradiation with femtosecond laser pulses as a function of laser fluence and distance from the laser irradiated region.

Figure 12 shows typical FESEM images of the debris formed around the irradiated region onto the sample surface by using fluences: 0.65 J/cm^2 (a) - (d), 0.41 J/cm^2 (e), (f) and 0.3 J/cm^2 (g), (h). Morphology of debris is found to be dependent on factors like fluence and distance from the irradiated region. With the increase of fluence more accumulation of debris is observed and the density of the debris is found to get decreased moving away from the microstructure. Figure 12(a) and 12(e) shows the debris distribution ~ 5 μm away from the microstructure fabricated with the fluence F = 0.65 and 0.41 J/cm^{-2}, indicating that the debris

are irregular sized particles and are composed of a continuous deposition of cotton-like aggregates containing few spherical shaped nanoparticles. Debris distribution ~ 20 µm away from the laser irradiated region with the fluence of F = 0.65 Jcm^{-2} is shown in figure 12(c), indicating that the density of debris decreases when moving away from the laser irradiated region and at the larger distance of ~ 50 µm away from the laser exposed region, isolated spherical shaped Si nanoparticles were observed. Under the irradiation with a lower fluence of F = 0.3 J/cm^2 no cotton-like debris were observed and due to scattering of ablated matter, debris in the form of isolated deposits of spherical shaped nanoparticles with dimensions ranging from 10 to 200 nm on the Si surface is observed as shown in figure 12(g). Figures 12(b), 12(d), 12(f) and 12(h) corresponds to high resolution images of 12(a), 12(c), 12(e) and 12(g) respectively.

The debris was collected onto a carbon-coated TEM grid by placing grids near the laser irradiated region. TEM analysis of the debris indicates that the larger particles accumulated around the laser irradiated region seemed as if they were formed with smaller aggregating particles as shown in figure 13. TEM images of debris obtained after irradiating with fluence F = 0.65 Jcm^{-2} and at a distance of ~ 5 and ~ 20 µm away from the microstructure is shown in figures 13(a) and 13(b). Figures 13(c) and 13(d) corresponds to the TEM images of debris obtained at a distance of ~ 5 µm away from the microstructures fabricated using a fluence of F = 0.41 and 0.3 J/cm^2 respectively. These nanoparticles possess a well-distinguished core-shell structure and can be observed from high-resolution images shown in figure 13(e) and 13(f). Formation of core-shell structure in Si nanoparticles obtained by fs laser irradiation of Si wafer in air is due to difference in heat transfer from inner and outer parts of nanoparticles to the surrounding environment. The cooling rate of the outer parts of the particles are higher than in the center, so the amorphous shell is formed, whereas the cooling rate inside the particle is low and a highly oriented crystalline structure is established.

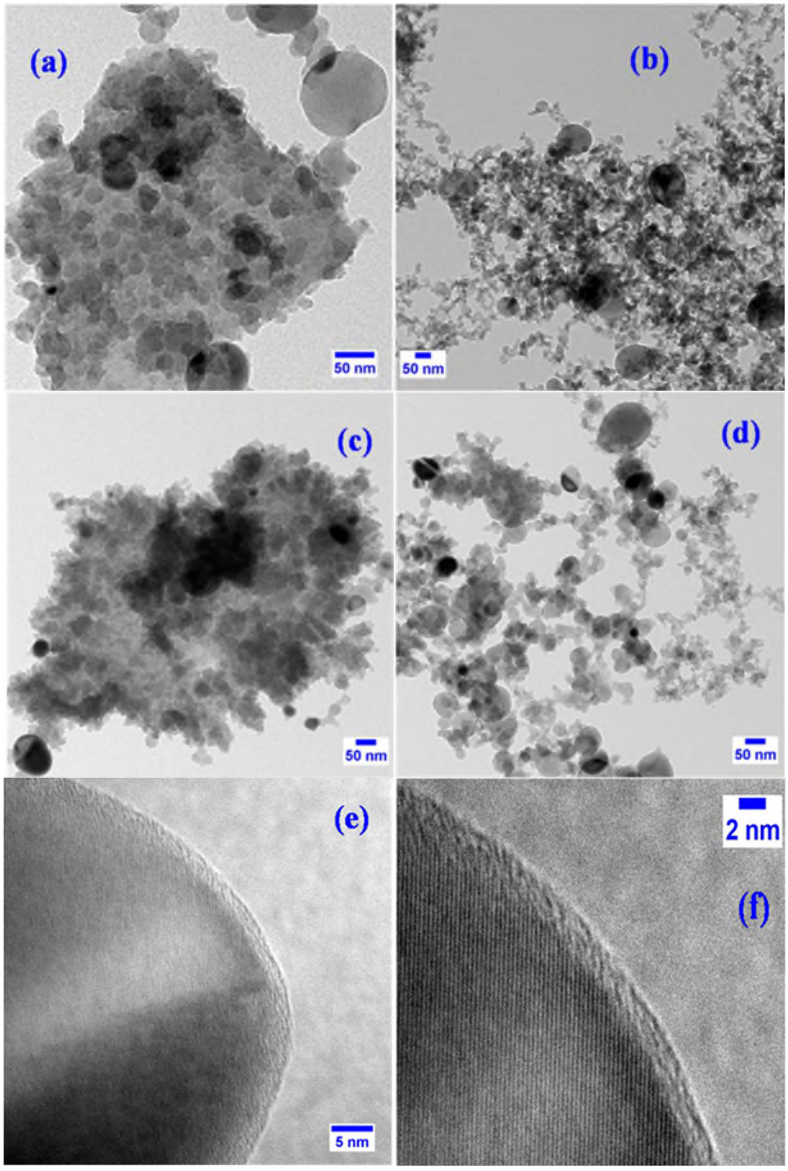

Figure 13: (a)- (d) TEM images showing the morphology of Si debris formed on the surface under irradiation with femtosecond laser pulses as a function of laser fluence and at different distances from the laser irradiated region. (e) and (f) shows formation core-shell Si nanoparticles in the collected debris.

The fs laser machining of the Si surface in air produced a significant amount of debris indicating that material is removed in the form of very small particles, such as small-scale clusters or atoms in the present laser irradiation conditions with fluence over the ablation threshold of 0.3 Jcm^{-2}. The ejected atoms and atomic clusters are formed to larger particle sizes in the range of 100 nm, aggregating to form cotton-like fragments on the solid substrate. TEM analysis of debris shown in figure 13 indicates that cotton-like aggregates are composed of small sized Si nanoparticles. The time sequence of the rounding, solidification, and

crystallization of the nanodroplet is considered as follows. Under fs laser irradiation with fluence well above the ablation threshold ablated matter is considered to be in a supercritical fluid state. During the cooling process, in hundreds of picoseconds duration a free liquid surface is formed after passing through the nucleation stage. This kind of rapid cooling, and hence the solidification, leads to the observed amorphization. In general, two kinds of amorphization of Si NPs were reported (i) complete amorphization of Si, which is particular for the particle, dimensions less than 10 nm and (ii) core−shell type in which amorphous silicon forms as shell on the crystalline Si core [54, 55]. Thus under fs laser irradiation surface layer of the Si is lifted up as a high temperature fluid, and finally decomposes into liquid fragments and the morphology and composition of the cooled liquid fragments depend on factors like laser fluence and distance from the irradiated region.

4. Conclusions

A detailed study is performed to understand the irradiation effects of intense 800 nm, 110 fs, 1 KHz laser pulses on single crystalline Si. Surface morphology has been studied as a function of various experimental parameters like fluence, number of laser pulses and polarization direction. HSFL structures aligned parallel to laser polarization direction with periods less than 320nm when Λ/λ less than 0.4 are formed at lower laser fluence of 0.22 J cm^{-2}. LSFL features appeared when the ratio Λ/λ is in between 0.4 and 1 with periods ranging from 320 to 800 nm. At a fluence of 0.26 Jcm^{-2}, coexistence of LSFL and HSFL are observed perpendicular and parallel to laser polarization directions respectively. At higher fluence, between 0.3 and 0.5 Jcm^{-2}, surface morphology depended on laser polarization, fluence and pulse number with formation of nanoparticles, subwavelength features (LSFL) and grooves. The orientation of LSFL is observed to be perpendicular to the incident laser polarization direction and it is independent of the scanning direction. With further increase in fluence to 0.65 Jcm^{-2}, few micrometer sized grains along with nanoparticles are seen all over the laser modified region. Non-thermal phase transition upon irradiation is observed with the excitation of electrons from valance to conduction band. Formation of LSFL depended on the laser fluence and also on the density of generated carriers in the conduction band. LIPSS is accompanied by the formation of Si NPs which again depended on the laser fluence. FESEM images depict spherical NPs and cotton like irregular shapes with sizes from 10 to 200 nm respectively at low and high fluences respectively. Raman scattering studies confirmed the formation of high pressure phases in the irradiated region. Strong luminescence in the visible

region is exhibited in the irradiated region due to the presence of large amount of oxidized Si NPs as confirmed by EDX analysis. Increase in oxygen to silicon ratio and luminescence intensity increased with laser fluence or applied number of pulses. Luminescence is not observed once the sample after etched with HF clearly indicates the emission due to the oxygen related defects. These significant results highlight the importance of the fabrication method adapted to achieve applications in various photonic technologies.

Conflict of interest: The authors declare that they have no conflict of interest.

References

1. D. Hirschman, L. Tsybeskov, S. P. Duttagupta, P. M. Fauchet “Silicon-based visible light-emitting devices integrated into microelectronic circuits” Nature 384 (1996) 338-341.
2. A. G. Cullis, L. T. Canham and P. D. J. Calcott “The structural and luminescence properties of porous silicon” Journal of Applied Physics 82, 909 (1997).
3. S. Pillai, K. R. Catchpole, T. Trupke, M. A. Green “Surface plasmon enhanced silicon solar cells” Journal of applied physics 101 (9), (2007) 093105.
4. W. Bai, Q. Gan, F. Bartoli, J. Zhang, L. Cai, Y. Huang, and G. Song “Design of plasmonic back structures for efficiency enhancement of thin-film amorphous Si solar cells” Optics Letters 34, (23) (2009) 3725-3727.
5. M. A. Green “The path to 25% silicon solar cell efficiency: History of silicon cell evolution” Progress in Photovoltaics: Research and Applications 17 (3), (2009) 183-189
6. S. S. Iyer and Y.-H. Xie “Light emission from silicon” Science 260 (5104), (1993) 40–46.
7. I. V. Anatova, M. B. Gulyaev, A. G. Cherkov, V. A. Volodin, D. V. Marin, V. A. Skuratov, J. Jedrzejewski, I. Balberg, “The modification of Si nanocrystallites embedded in a dielectric matrix by high energy ion irradiation” Nanotechnology 20 (2009) 095205.
8. G. Kurumurthy, K. S. Alee, D. N. Rao “Photoluminescence studies of Si/SiO_2 nanoparticles synthesized with different laser irradiation wavelengths of nanosecond pulse duration” Optics communications 282 (17), 3509-3512.
9. L. Pavesi, L. Dal Negro, C. Mazzoleni, G. Franzò, and F. Priolo, “Optical gain in silicon nanocrystals” Nature 408, (2000) 440–444.

10. R. Kuladeep, M. H. Dar, K. L. N. Deepak, D. N. Rao “Ultrafast laser induced periodic sub-wavelength aluminum surface structures and nanoparticles in air and liquids” Journal of Applied Physics 116 (11), (2014) 113107.
11. S. Xu, R. Ding, C. Yao, H. Liu, Y. Wan, J. Wang, Y. Ye, X. Yuan “Effects of pulse durations and environments on femtosecond laser ablation of stainless steel” Appl. Phys. A 124, (2018) 310.
12. S. K. Das, A. Andreev, H. Messaoudi, J. Braenzel, M. Schnuerer, R. Grunwald “Highly periodic laser-induced nanostructures on thin Ti and Cu foils for potential application in laser ion acceleration” Journal of Applied Physics 119 (11), (2016) 113101.
13. C. S. R. Nathala, A. Ajami, A. A. Ionin, S. I. Kudryashov, S. V. Makarov, T. Ganz, A. Assion and W. Husinsky “Experimental study of fs-laser induced sub-100-nm periodic surface structures on titanium” Optics Express 23, (2015) 5915-5929.
14. G. Miyaji and K. Miyazaki “Nanoscale ablation on patterned diamondlike carbon film with femtosecond laser pulses” Applied Physics Letters 91 (2007) 123102.
15. S. K. Das, H. Messaoudi, A. Debroy, E. McGlynn, R. Grunwald “Multiphoton excitation of surface plasmon-polaritons and scaling of nanoripple formation in large bandgap materials” Optical Materials Express 3 (10), (2013) 1705-1715.
16. K. Sugioka, Y. Cheng “Ultrafast lasers—reliable tools for advanced materials processing” Light Sci. Appl. 3, (2014) e149.
17. Y. Liao, Y. Ju, L. Zhang, F. He, Q. Zhang, Y. Shen, D. Chen, Y. Cheng, Z. Xu, K. Sugioka, and K. Midorikawa “Three-dimensional microfluidic channel with arbitrary length and configuration fabricated inside glass by femtosecond laser direct writing” Optics Letters 35, (2010) 3225-3227.
18. D. Wu, Q. D. Chen, L. G. Niu, J. N. Wang, J. Wang, R. Wang, H. Xia, H. Sun “Femtosecond laser rapid prototyping of nanoshells and suspending components towards microfluidic devices” Lab Chip 9, (2009) 2391–2394.
19. M. H. Dar, R. Kuladeep, V. Saikiran, D. N. Rao, “Femtosecond laser nanostructuring of titanium metal towards fabrication of low-reflective surfaces over broad wavelength range” Applied Surface Science 371, (2016) 479-487.
20. Q. K. Li, J. J. Cao, Y. H. Yu, L. Wang, Y. L. Sun, Q.D. Chen, and H. B. Sun, “Fabrication of an anti-reflective microstructure on sapphire by femtosecond laser direct writing” Optics Letters 42, (2017) 543–546.
21. A. Y. Vorobyev and C. Guo “Colorizing metals with femtosecond laser pulses” Appl. Phys. Lett. 92, (2008) 041914.

22. V. Parmar, P. K. Kanaujia, R. K. Bommali, G. V. Prakash “Efficient Surface Enhanced Raman Scattering substrates from femtosecond laser based fabrication” Optical Materials 72, (2017), 86-90.
23. X. Tan, L. Jiang, J. Hu, P. Liu, A. Wang, and Y. Lu “Highly sensitive and homogeneous SERS substrate fabricated by a femtosecond laser combined with dewetting” Chinese Optics Letters 13, (2015) 111401.
24. G. K. Podagatlapalli, S. Hamad, S. P. Tewari, S. Sreedhar, M. D. Prasad, S. V. Rao “Silver nano-entities through ultrafast double ablation in aqueous media for surface enhanced Raman scattering and photonics applications” Journal of Applied Physics 113 (7), (2013) 073106.
25. Q. Q. Yang, X. Li, L. Jiang, N. Zhang, G. M. Zhang, X. S. Shi, K. H. Zhang, J. Hu, and Y. F. Lu, “Nanopillar arrays with nanoparticles fabricated by a femtosecond laser pulse train for highly sensitive SERRS” Opt. Lett. 40, (2015) 2045.
26. I. Gnilitskyi, V. Gruzdev, N. M. Bulgakova, T. Mocek, and L. Orazi “Mechanisms of high-regularity periodic structuring of silicon surface by sub-MHz repetition rate ultrashort laser pulses” Applied Physics Letters 109, (2016) 143101.
27. D. Zhang and K. Sugioka “Hierarchical microstructures with high spatial frequency laser induced periodic surface structures possessing different orientations created by femtosecond laser ablation of silicon in liquids” Opto Electronic Advances 2, (2019) 190002.
28. V. Parmar, Y. C. Shin “Wideband anti-reflective silicon surface structures fabricated by femtosecond laser texturing” Applied Surface Science 459, (2018) 86-91.
29. Q. Zhu & M. Shen “Femtosecond laser irradiation-induced infrared absorption on silicon surfaces” International Journal of Smart and Nano Materials, 6:2, (2015) 113-123. https://doi.org/10.1080/19475411.2015.1057268
30. J. Bonse, and J. Krüger “Pulse number dependence of laser-induced periodic surface structures for femtosecond laser irradiation of silicon” Journal of Applied Physics 108, (2010) 034903.
31. A. Hamdorf, M. Olson, C-H Lin, L. Jiang, J. Zhou, H. Xiao, and H-L Tsai “Femtosecond and nanosecond laser fabricated substrate for surface-enhanced Raman scattering” Optics Letters 36, (2011) 3353.
32. T. J.-Y. Derrien, R. Koter, J. Krüger, S. Höhm, A. Rosenfeld, and J. Bonse, “Plasmonic formation mechanism of periodic 100-nm-structures upon femtosecond laser irradiation of silicon in water” Journal of Applied Physics. 116, (2014) 074902.

33. J. J. J. Nivas, K. K. Anoop, R. Bruzzese, R. Philip, S. Amoruso “Direct femtosecond laser surface structuring of crystalline silicon at 400 nm” Appl. Phys. Lett. 112, (2018) 121601.
34. R. Kuladeep, C. Sahoo, and D. N. Rao, “Direct writing of continuous and discontinuous sub-wavelength periodic surface structures on single-crystalline silicon using femtosecond laser” Applied Physics Letters. 104, (2014) 222103.
35. S. Lee, K. Jo, H. Keum, S. Chae, Y. Kim, J. Choi, H. H. Leec, H. J. Kim “Nanowall formation by maskless wet-etching on a femtosecond laser irradiated silicon surface” Applied Surface Science 437 (2018) 190–194.
36. J. J. J. Nivas, Z. Song, R. Fittipaldi, A. Vecchione, R. Bruzzese, S. Amoruso “Direct ultrashort laser surface structuring of silicon in air and vacuum at 1055 nm” Applied Surface Science 417, (2017) 149-154.
37. A. A. Ionin, S. I. Kudryashov, A. A. Rudenko, L. V. Seleznev, D. V. Sinitsyn, D. V. Sinitsyn and S. V. Makarov “Nonlinear optical feedback for nano- and micropatterning of silicon surface under femtosecond laser irradiation” Optical Material Express 7(8), (2017) 2793.
38. A. A. Ionin, S. I. Kudryashov, A. O. Levchenko, L. V. Nguyen, I. N. Saraeva, A. A. Rudenko, A. A. Ageev, D. V. Potorochin, V. P. Veiko, E. V. Borisov, D. V. Pankin, D. A. Kirilenko, P. N. Brunkov “Correlated topographic and structural modification on Si surface during multi-shot femtosecond laser exposures: Si nanopolymorphs as potential local structural nanomarkers” Applied Surface Science 416, (2017) 988-995.
39. J. J. J. Nivas, H. Shutong, K. K. Anoop, A. Rubano, R. Fittipaldi, A. Vecchione, D. Paparo, L. Marrucci, R. Bruzzese, and S. Amoruso “ Laser ablation of silicon induced by a femtosecond optical vortex beam” Optics Letters 40, 20, (2015) 4611-4614.
40. K. Itoh, W. Watanabe, S. Nolte and C.B. Schaffer “Ultrafast Processes for Bulk Modification of Transparent Materials” MRS Bull. 31 (2006) 620-625.
41. K. S. Tinten and D. V. Linde “Generation of dense electron-hole plasmas in silicon” Physical Review B. 61, (2000) 2643-2650.
42. J. Bonse, A. Rosenfeld, and J. Kruger “On the role of surface plasmon polaritons in the formation of laser-induced periodic surface structures upon irradiation of silicon by femtosecond-laser pulses” Journal of Applied Physics. 106, (2009) 104910.
43. S. K. Sundaram and E. Mazur “Inducing and probing non-thermal transitions in semiconductors using femtosecond laser pulses” Nature materials 1, (2002) 217- 224.

44. M. Huang, F. Zhao, Y. Cheng, N. Xu and Z. Xu, “Origin of Laser-Induced Near-Subwavelength Ripples: Interference between Surface Plasmons and Incident Laser” ACS Nano. 3, (2009) 4062- 4070.
45. S. Sakabe, M. Hashida, S. Tokita, S. Namba and K. Okamuro “Mechanism for self-formation of periodic grating structures on a metal surface by a femtosecond laser pulse” Physical Review B. 79, (2009) 033409.
46. A. Borowiec and H. K. Haugen “Subwavelength ripple formation on the surfaces of compound semiconductors irradiated with femtosecond laser pulses” Applied Physics Letters 82, (2003) 4462.
47. S. Amoruso, R. Bruzzese, N. Spinelli, R. Velotta, M. Vitiello, X. Wang, G. Ausanio, V. Iannotti and L. Lanotte “Generation of silicon nanoparticles via femtosecond laser ablation in vacuum” Applied Physics Letters. 84, (2004) 4502.
48. D. Scuderi, O. Albert, D. Moreau, P. P. Pronko and J. Etchepare “Interaction of a laser-produced plume with a second time delayed femtosecond pulse” Applied Physics Letters. 86, (2005) 071502.
49. T.J.-Y. Derrien, R. Torres, T. Sarnet, M. Sentis and T. E. Itina, “Formation of femtosecond laser induced surface structures on silicon: Insights from numerical modeling and single pulse experiments” Applied Surface Science. 258, (2012) 9487–9490.
50. G. Miyaji, K. Miyazaki, K. Zhang, T. Yoshifuji and J. Fujita “Mechanism of femtosecond-laser-induced periodic nanostructure formation on crystalline silicon surface immersed in water” Optics Express. 20, (2012) 14848-14856.
51. U. Chakravarty, P. A. Naik, J. A. Chakera, A. Upadhyay and P. D. Gupta “Estimation of electron density and temperature of semiconductor surfaces excited by ultra-short laser pulses” Appl. Phys. A 115, (2014) 1457–1467.
52. J. V. Obona, J. Z. P. Skolski, G. R. B. E. Romer, and A. J. Huis in `t Veld “Pulse-analysis-pulse investigation of femtosecond laser-induced periodic surface structures on silicon in air” Optics Express. 22, (2014) 9254- 9261.
53. J. Bonse, S. Baudach, J. Krüger, W. Kautek, M. Lenzner “Femtosecond laser ablation of silicon–modification thresholds and morphology” Appl. Phys. A 74, (2002) 19.
54. T. E. Glover, Hydrodynamics of particle formation following femtosecond laser ablation” J. Opt. Soc. Am. B. 20 (2003) 125-131.
55. Y. Kanemitsu, I. Nakada and H. Kuroda “Picosecond laser induced anomalous crystallization in amorphous silicon” Applied Physics Letters. 47, (1985) 939.

56. J. P. Wilcoxon, G. A. Samara “Tailorable, visible light emission from silicon nanocrystals” Appl. Phys. Lett. 74, (1999) 3164.
57. J. Zi, K. Zhang, X. Xie “Comparison of models for Raman spectra of Si nanocrystals” Phys. Rev. B 55, (1997) 9263.
58. A. Alessi, S. Agnello, G. Buscarino and F. M. Gelardi “Structural properties of core and surface of silica nanoparticles investigated by Raman spectroscopy” Journal of Raman Spectrosc. 44, (2013) 810–816.
59. M. Schade, O. Varlamova, J. Reif, H. Blumtritt, W. Erfurth, and H.S. Leipner “High-resolution investigations of ripple structures formed by femtosecond laser irradiation of silicon” Anal. Bioanal. Chem. 396 (2010), 1905–1911.
60. C. Smit, R. A. C. M. M. van Swaaij, H. Donker, A. M. H. N. Petit, W. M. M. Kessels, and M. C. M. van de Sanden “Determining the material structure of microcrystalline silicon from Raman spectra” Journal of Applied Physics. 94, (2003) 3582.
61. Y. Izawa, Y. Izawa, Y. Setsuhara, M. Hashida, M. Fujita, R. Sasaki, H. Nagai and M. Yoshida “Ultrathin amorphous Si layer formation by femtosecond laser pulse irradiation” Applied Physics Letters. 90, (2007) 044107.
62. P. P. Dey and A. Khare “Fabrication of luminescent a-Si:SiO2 structures by direct irradiation of high power laser on silicon surface” Applied Surface Science. 307, (2014) 77–85.
63. C. Wu, C. H. Crouch, L. Zhao, and E. Mazur “Visible luminescence from silicon surfaces microstructured in air” Applied Physics Letters. 81, (2002) 1999.
64. T. Chen, J. Si, X. Hou, S. Kanehira, K. Miura and K. Hirao “Luminescence of black silicon fabricated by high-repetition rate femtosecond laser pulses” Journal of Applied Physics. 110, (2011) 073106.
65. Y. S. Liu, S. W. Chiang and F. Bacon “Rapid oxidation via adsorption of oxygen in laser-induced amorphous silicon” Applied Physics Letters. 38, (1981) 1005.
66. E. Fogarassy, C. W. White, A. Slaoui, C. Fuchs, P. Siffert and S. J. Pennycook “Excimer laser induced oxidation of ion-implanted silicon” Applied Physics Letters. 53, (1988) 1720.
67. Koichiro, H. Koyama, K. Uda and Y. Miura “Incorporation of Oxygen into Silicon during Pulsed-Laser Irradiation" Japanese journal of applied physics. 19, (1980) 375-378.

Optical, structural and morphological studies of nanostructures fabricated on silicon surface by femtosecond laser irradiation

Kuladeep, Rajamudili

2022-01-03

Rajamudili K, Jyothi L, Sahoo C, et al., (2022) Optical, structural and morphological studies of nanostructures fabricated on silicon surface by femtosecond laser irradiation. Journal of Materials Science, Volume 57, Issue 3, January 2022, pp. 1863-1880

https://doi.org/10.1007/s10853-021-06712-5